Eur. Phys. J. C 46, 277–293 (2006)
Digital Object Identifier (DOI) 10.1140/epjc/s2006-02501-3

THE EUROPEAN PHYSICAL JOURNAL C

Search for excited leptons in e^+e^- collisions at $\sqrt{s} = 189-209\,\mathrm{GeV}$

The DELPHI Collaboration

J. Abdallah[25], P. Abreu[22], W. Adam[51], P. Adzic[11], T. Albrecht[17], T. Alderweireld[2], R. Alemany-Fernandez[8], T. Allmendinger[17], P.P. Allport[23], U. Amaldi[29], N. Amapane[45], S. Amato[48], E. Anashkin[36], A. Andreazza[28], S. Andringa[22], N. Anjos[22], P. Antilogus[25], W.-D. Apel[17], Y. Arnoud[14], S. Ask[26], B. Asman[44], J.E. Augustin[25], A. Augustinus[8], P. Baillon[8], A. Ballestrero[46], P. Bambade[20], R. Barbier[27], D. Bardin[16], G.J. Barker[17], A. Baroncelli[39], M. Battaglia[8], M. Baubillier[25], K.-H. Becks[53], M. Begalli[6], A. Behrmann[53], E. Ben-Haim[20], N. Benekos[32], A. Benvenuti[5], C. Berat[14], M. Berggren[25], L. Berntzon[44], D. Bertrand[2], M. Besancon[40], N. Besson[40], D. Bloch[9], M. Blom[31], M. Bluj[52], M. Bonesini[29], M. Boonekamp[40], P.S.L. Booth[23], G. Borisov[21], O. Botner[49], B. Bouquet[20], T.J.V. Bowcock[23], I. Boyko[16], M. Bracko[43], R. Brenner[49], E. Brodet[35], P. Bruckman[18], J.M. Brunet[7], L. Bugge[33], P. Buschmann[53], M. Calvi[29], T. Camporesi[8], V. Canale[38], F. Carena[8], N. Castro[22], F. Cavallo[5], M. Chapkin[42], P. Charpentier[8], P. Checchia[36], R. Chierici[8], P. Chliapnikov[42], J. Chudoba[8], S.U. Chung[8], K. Cieslik[18], P. Collins[8], R. Contri[13], G. Cosme[20], F. Cossutti[47], M.J. Costa[50], D. Crennell[37], J. Cuevas[34], J. D'Hondt[2], J. Dalmau[44], T. da Silva[48], W. Da Silva[25], G. Della Ricca[47], A. De Angelis[47], W. De Boer[17], C. De Clercq[2], B. De Lotto[47], N. De Maria[45], A. De Min[36], L. de Paula[48], L. Di Ciaccio[38], A. Di Simone[39], K. Doroba[52], J. Drees[53,8], M. Dris[32], G. Eigen[4], T. Ekelof[49], M. Ellert[49], M. Elsing[8], M.C. Espirito Santo[22], G. Fanourakis[11], D. Fassouliotis[11,3], M. Feindt[17], J. Fernandez[41], A. Ferrer[50], F. Ferro[13], U. Flagmeyer[53], H. Foeth[8], E. Fokitis[32], F. Fulda-Quenzer[20], J. Fuster[50], M. Gandelman[48], C. Garcia[50], P. Gavillet[8], E. Gazis[32], R. Gokieli[8,52], B. Golob[43], G. Gomez-Ceballos[41], P. Goncalves[22], E. Graziani[39], G. Grosdidier[20], K. Grzelak[52], J. Guy[37], C. Haag[17], A. Hallgren[49], K. Hamacher[53], K. Hamilton[35], S. Haug[33], F. Hauler[17], V. Hedberg[26], M. Hennecke[17], H. Herr[8], J. Hoffman[52], S.-O. Holmgren[44], P.J. Holt[8], M.A. Houlden[23], K. Hultqvist[44], J.N. Jackson[23], G. Jarlskog[26], P. Jarry[40], D. Jeans[35], E.K. Johansson[44], P.D. Johansson[44], P. Jonsson[27], C. Joram[8], L. Jungermann[17], F. Kapusta[25], S. Katsanevas[27], E. Katsoufis[32], G. Kernel[43], B.P. Kersevan[8,43], U. Kerzel[17], A. Kiiskinen[15], B.T. King[23], N.J. Kjaer[8], P. Kluit[31], P. Kokkinias[11], C. Kourkoumelis[3], O. Kouznetsov[16], Z. Krumstein[16], M. Kucharczyk[18], J. Lamsa[1], G. Leder[51], F. Ledroit[14], L. Leinonen[44], R. Leitner[30], J. Lemonne[2], V. Lepeltier[20], T. Lesiak[18], W. Liebig[53], D. Liko[51], A. Lipniacka[44], J.H. Lopes[48], J.M. Lopez[34], D. Loukas[11], P. Lutz[40], L. Lyons[35], J. MacNaughton[51], A. Malek[53], S. Maltezos[32], F. Mandl[51], J. Marco[41], R. Marco[41], B. Marechal[48], M. Margoni[36], J.-C. Marin[8], C. Mariotti[8], A. Markou[11], C. Martinez-Rivero[41], J. Masik[12], N. Mastroyiannopoulos[11], F. Matorras[41], C. Matteuzzi[29], F. Mazzucato[36], M. Mazzucato[36], R. Mc Nulty[23], C. Meroni[28], E. Migliore[45], W. Mitaroff[51], U. Mjoernmark[26], T. Moa[44], M. Moch[17], K. Moenig[8,10], R. Monge[13], J. Montenegro[31], D. Moraes[48], S. Moreno[22], P. Morettini[13], U. Mueller[53], K. Muenich[53], M. Mulders[31], L. Mundim[6], W. Murray[37], B. Muryn[19], G. Myatt[35], T. Myklebust[33], M. Nassiakou[11], F. Navarria[5], K. Nawrocki[52], R. Nicolaidou[40], M. Nikolenko[16,9], A. Oblakowska-Mucha[19], V. Obraztsov[42], A. Olshevski[16], A. Onofre[22], R. Orava[15], K. Osterberg[15], A. Ouraou[40], A. Oyanguren[50], M. Paganoni[29], S. Paiano[5], J.P. Palacios[23], H. Palka[18], T.D. Papadopoulou[32], L. Pape[8], C. Parkes[24], F. Parodi[13], U. Parzefall[8], A. Passeri[39], O. Passon[53], L. Peralta[22], V. Perepelitsa[50], A. Perrotta[5], A. Petrolini[13], J. Piedra[41], L. Pieri[39], F. Pierre[40], M. Pimenta[22], E. Piotto[8], T. Podobnik[43], V. Poireau[8], M.E. Pol[6], G. Polok[18], V. Pozdniakov[16], N. Pukhaeva[2,16], A. Pullia[29], J. Rames[12], A. Read[33], P. Rebecchi[8], J. Rehn[17], D. Reid[31], R. Reinhardt[53], P. Renton[35], F. Richard[20], J. Ridky[12], M. Rivero[41], D. Rodriguez[41], A. Romero[45], P. Ronchese[36], P. Roudeau[20], T. Rovelli[5], V. Ruhlmann-Kleider[40], D. Ryabtchikov[42], A. Sadovsky[16], L. Salmi[15], J. Salt[50], C. Sander[17], A. Savoy-Navarro[25], U. Schwickerath[8], A. Segar[35], R. Sekulin[37], M. Siebel[53], A. Sisakian[16], G. Smadja[27], O. Smirnova[26], A. Sokolov[42], A. Sopczak[21], R. Sosnowski[52], T. Spassov[8], M. Stanitzki[17], A. Stocchi[20], J. Strauss[51], B. Stugu[4], M. Szczekowski[52], M. Szeptycka[52], T. Szumlak[19], T. Tabarelli[29], A.C. Taffard[23], F. Tegenfeldt[49], J. Timmermans[31], L. Tkatchev[16], M. Tobin[23], S. Todorovova[12], B. Tome[22], A. Tonazzo[29], P. Tortosa[50], P. Travnicek[12], D. Treille[8], G. Tristram[7], M. Trochimczuk[52], C. Troncon[28], M.-L. Turluer[40], I.A. Tyapkin[16], P. Tyapkin[16], S. Tzamarias[11], V. Uvarov[42], G. Valenti[5], P. Van Dam[31], J. Van Eldik[8], A. Van Lysebetten[2], N. van Remortel[2], I. Van Vulpen[8], G. Vegni[28], F. Veloso[22], W. Venus[37], P. Verdier[27], V. Verzi[38], D. Vilanova[40], L. Vitale[47], V. Vrba[12], H. Wahlen[53], A.J. Washbrook[23], C. Weiser[17], D. Wicke[8], J. Wickens[2], G. Wilkinson[35], M. Winter[9], M. Witek[18], O. Yushchenko[42], A. Zalewska[18], P. Zalewski[52], D. Zavrtanik[43], V. Zhuravlov[16], N.I. Zimin[16], A. Zintchenko[16], M. Zupan[11]

[1] Department of Physics and Astronomy, Iowa State University, Ames, IA 50011-3160, USA
[2] Physics Department, Universiteit Antwerpen, Universiteitsplein 1, 2610 Antwerpen, Belgium
and IIHE, ULB-VUB, Pleinlaan 2, 1050 Brussels, Belgium
and Faculté des Sciences, Univ. de l'Etat Mons, Av. Maistriau 19, 7000 Mons, Belgium
[3] Physics Laboratory, University of Athens, Solonos Str. 104, 10680 Athens, Greece
[4] Department of Physics, University of Bergen, Allégaten 55, 5007 Bergen, Norway
[5] Dipartimento di Fisica, Università di Bologna and INFN, Via Irnerio 46, 40126 Bologna, Italy
[6] Centro Brasileiro de Pesquisas Físicas, rua Xavier Sigaud 150, 22290 Rio de Janeiro, Brazil
and Depto. de Física, Pont. Univ. Católica, C.P. 38071 22453 Rio de Janeiro, Brazil
and Inst. de Física, Univ. Estadual do Rio de Janeiro, rua São Francisco Xavier 524, Rio de Janeiro, Brazil
[7] Collège de France, Lab. de Physique Corpusculaire, IN2P3-CNRS, 75231 Paris Cedex 05, France
[8] CERN, 1211 Geneva 23, Switzerland
[9] Institut de Recherches Subatomiques, IN2P3 – CNRS/ULP – BP20, 67037 Strasbourg Cedex, France
[10] Now at DESY-Zeuthen, Platanenallee 6, 15735 Zeuthen, Germany
[11] Institute of Nuclear Physics, N.C.S.R. Demokritos, P.O. Box 60228, 15310 Athens, Greece
[12] FZU, Inst. of Phys. of the C.A.S. High Energy Physics Division, Na Slovance 2, 180 40, Praha 8, Czech Republic
[13] Dipartimento di Fisica, Università di Genova and INFN, Via Dodecaneso 33, 16146 Genova, Italy
[14] Institut des Sciences Nucléaires, IN2P3-CNRS, Université de Grenoble 1, 38026 Grenoble Cedex, France
[15] Helsinki Institute of Physics, P.O. Box 64, 00014 University of Helsinki, Finland
[16] Joint Institute for Nuclear Research, Dubna, Head Post Office, P.O. Box 79, 101 000 Moscow, Russian Federation
[17] Institut für Experimentelle Kernphysik, Universität Karlsruhe, Postfach 6980, 76128 Karlsruhe, Germany
[18] Institute of Nuclear Physics PAN,Ul. Radzikowskiego 152, 31142 Krakow, Poland
[19] Faculty of Physics and Nuclear Techniques, University of Mining and Metallurgy, 30055 Krakow, Poland
[20] Université de Paris-Sud, Lab. de l'Accélérateur Linéaire, IN2P3-CNRS, Bât. 200, 91405 Orsay Cedex, France
[21] School of Physics and Chemistry, University of Lancaster, Lancaster LA1 4YB, UK
[22] LIP, IST, FCUL - Av. Elias Garcia, 14-1o, 1000 Lisboa Codex, Portugal
[23] Department of Physics, University of Liverpool, P.O. Box 147, Liverpool L69 3BX, UK
[24] Dept. of Physics and Astronomy, Kelvin Building, University of Glasgow, Glasgow G12 8QQ, UK.
[25] LPNHE, IN2P3-CNRS, Univ. Paris VI et VII, Tour 33 (RdC), 4 place Jussieu, 75252 Paris Cedex 05, France
[26] Department of Physics, University of Lund, Sölvegatan 14, 223 63 Lund, Sweden
[27] Université Claude Bernard de Lyon, IPNL, IN2P3-CNRS, 69622 Villeurbanne Cedex, France
[28] Dipartimento di Fisica, Università di Milano and INFN-MILANO, Via Celoria 16, 20133 Milan, Italy
[29] Dipartimento di Fisica, Univ. di Milano-Bicocca and INFN-MILANO, Piazza della Scienza 2, 20126 Milan, Italy
[30] IPNP of MFF, Charles Univ., Areal MFF, V Holesovickach 2, 180 00, Praha 8, Czech Republic
[31] NIKHEF, Postbus 41882, 1009 DB Amsterdam, The Netherlands
[32] National Technical University, Physics Department, Zografou Campus, 15773 Athens, Greece
[33] Physics Department, University of Oslo, Blindern, 0316 Oslo, Norway
[34] Dpto. Fisica, Univ. Oviedo, Avda. Calvo Sotelo s/n, 33007 Oviedo, Spain
[35] Department of Physics, University of Oxford, Keble Road, Oxford OX1 3RH, UK
[36] Dipartimento di Fisica, Università di Padova and INFN, Via Marzolo 8, 35131 Padua, Italy
[37] Rutherford Appleton Laboratory, Chilton, Didcot OX11 OQX, UK
[38] Dipartimento di Fisica, Università di Roma II and INFN, Tor Vergata, 00173 Rome, Italy
[39] Dipartimento di Fisica, Università di Roma III and INFN, Via della Vasca Navale 84, 00146 Rome, Italy
[40] DAPNIA/Service de Physique des Particules, CEA-Saclay, 91191 Gif-sur-Yvette Cedex, France
[41] Instituto de Fisica de Cantabria (CSIC-UC), Avda. los Castros s/n, 39006 Santander, Spain
[42] Inst. for High Energy Physics, Serpukov P.O. Box 35, Protvino, (Moscow Region), Russian Federation
[43] J. Stefan Institute, Jamova 39, 1000 Ljubljana, Slovenia
and Laboratory for Astroparticle Physics, Nova Gorica Polytechnic, Kostanjeviska 16a, 5000 Nova Gorica, Slovenia
and Department of Physics, University of Ljubljana, 1000 Ljubljana, Slovenia
[44] Fysikum, Stockholm University, Box 6730, 113 85 Stockholm, Sweden
[45] Dipartimento di Fisica Sperimentale, Università di Torino and INFN, Via P. Giuria 1, 10125 Turin, Italy
[46] INFN, Sezione di Torino, and Dipartimento di Fisica Teorica, Università di Torino, Via P. Giuria 1, 10125 Turin, Italy
[47] Dipartimento di Fisica, Università di Trieste and INFN, Via A. Valerio 2, 34127 Trieste, Italy
and Istituto di Fisica, Università di Udine, 33100 Udine, Italy
[48] Univ. Federal do Rio de Janeiro, C.P. 68528 Cidade Univ., Ilha do Fundão 21945-970 Rio de Janeiro, Brazil
[49] Department of Radiation Sciences, University of Uppsala, P.O. Box 535, 751 21 Uppsala, Sweden
[50] IFIC, Valencia-CSIC, and D.F.A.M.N., U. de Valencia, Avda. Dr. Moliner 50, 46100 Burjassot (Valencia), Spain
[51] Institut für Hochenergiephysik, Österr. Akad. d. Wissensch., Nikolsdorfergasse 18, 1050 Vienna, Austria
[52] Inst. Nuclear Studies and University of Warsaw, Ul. Hoza 69, 00681 Warsaw, Poland
[53] Fachbereich Physik, University of Wuppertal, Postfach 100 127, 42097 Wuppertal, Germany

Received: 11 January 2005 / Revised version: 19 January 2006 /
Published online: 31 March 2006 –

Abstract. A search for excited lepton production in e^+e^- collisions was performed using the data collected by the DELPHI detector at LEP at centre-of-mass energies ranging from 189 GeV to 209 GeV, corresponding to an integrated luminosity of approximately 600 pb^{-1}. No evidence for excited lepton production was found. In searches for pair-produced excited leptons, lower mass limits were established in the range 94–103 GeV/c^2, depending on the channel and model assumptions. In searches for singly-produced excited leptons, upper limits on the parameter f/Λ were established as a function of the mass.

1 Introduction

Excited leptons are predicted by models with substructure in the fermionic sector [1–3]. They are assumed to have spin and weak isospin equal to 1/2 and to have both their left-handed and right-handed components arranged in weak isodoublets:

$$L_L^* = \begin{pmatrix} \nu^* \\ \ell^* \end{pmatrix}_L \quad L_R^* = \begin{pmatrix} \nu^* \\ \ell^* \end{pmatrix}_R$$

where $\nu^* = \nu_e^*, \nu_\mu^*, \nu_\tau^*$ and $\ell^* = e^*, \mu^*, \tau^*$ represent the different flavours of neutral and charged excited leptons respectively. Excited leptons ($L^* \equiv \ell^*, \nu^*$) couple to the photon and/or to the $\mathrm{W}^\pm$ and Z^0 gauge bosons according to their quantum numbers and thus could be pair produced at LEP. Single production in association with their Standard Model (SM) partners ($L \equiv \ell, \nu$) would also be possible and its cross-sections would depend on the LL^*V couplings ($V \equiv \gamma, \mathrm{W}^\pm, \mathrm{Z}^0$) [4]. Excited leptons with masses up to the centre-of-mass energy ($\sqrt{s}$) can be searched for through the single-production mode.

This paper presents results of a search for single and pair production of excited leptons of all flavours using data collected by the DELPHI experiment at LEP at centre-of-mass energies between 189 GeV and 209 GeV. Previous results by DELPHI and the other LEP experiments can be found in [5–7], while results from the HERA experiments can be found in [8]. The paper is organised as follows: section 2 reviews the phenomenology of excited-lepton production and decay and its consequences for the experimental strategy; in Sect. 3 a detector overview is given and the data and Monte Carlo simulations are presented; event selection criteria applied to the different search channels are described in Sect. 4 and the results obtained are presented in Sect. 5; finally, a summary is presented in Sect. 6.

2 Production and decay of excited leptons

Pair production of charged excited leptons in e^+e^- collisions proceeds via s-channel γ and Z^0 exchanges, while for excited neutrinos only the Z^0 diagram contributes (Fig. 1). Pair production of excited electrons or excited electron neutrinos is also possible through t-channel exchange diagrams. In this case two LL^*V vertices are involved and the contribution to the total production cross-section is expected to be negligible compared to the s-channel exchange diagrams.

Single excited-lepton production arises from s-channel photon and Z^0 exchange (Fig. 1). Important additional contributions from t-channel γ and Z^0 exchange arise for excited electron production, while t-channel $\mathrm{W}^\pm$ exchange can be important for the excited electron neutrino. In the t-channel production of excited electrons, the SM spectator electron is emitted at small angles to the colliding beams direction and thus is often not detected.

The $\mathrm{SU}(2) \times \mathrm{U}(1)$ gauge-invariant effective Lagrangian describing the magnetic transition between excited leptons and the SM leptons has the form [3]:

$$\mathcal{L}_{LL^*} = \frac{1}{2\Lambda}\overline{L^*}\sigma^{\mu\nu}\left[gf\frac{\overrightarrow{\tau}}{2}\cdot\overrightarrow{W}_{\mu\nu} + g'f'\frac{Y}{2}B_{\mu\nu}\right]L_L + \text{hermitian conjugate}$$

where $L^* = L_L^* + L_R^*$ and L_L is the weak isodoublet with the left-handed components of the SM leptons; $\sigma^{\mu\nu}$ is the covariant bilinear tensor, $\overrightarrow{\tau}$ are the Pauli matrices, Y is the weak hypercharge, $\overrightarrow{W}_{\mu\nu}$ and $B_{\mu\nu}$ represent the gauge field tensors of SU(2) and U(1) respectively, with g and g' being the corresponding SM coupling constants; the parameter Λ sets the compositeness scale, with f and f' being weight factors associated with the two gauge groups. This Lagrangian is associated to the LL^*V vertex, and describes the single production of excited leptons and their decay branching ratios radiating a photon or a $\mathrm{W}^\pm$ or Z^0 boson. The strength of the LL^*V coupling is parameterised through f and f'. Form factors and anomalous magnetic moments of the excited leptons were not considered in the reported analyses. To reduce the number of free parameters it is customary to consider a relation between f and f', or set one of the parameters to zero. In this paper the relations $f = f'$ and $f = -f'$ are assumed. With the assumption $|f| = |f'|$, the single excited-lepton production cross-section depends only on the ratio f/Λ and on the excited-lepton mass.

Excited leptons with masses above 20 GeV/c^2 are assumed to decay promptly by radiating a photon, $\mathrm{W}^\pm$ or Z^0 boson. Their mean lifetime is predicted to be less than 10^{-15} s in all the studied scenarios. Thus, for detection purposes, excited leptons essentially decay at the production point. The decay branching ratios are function of the f and f' parameters, as shown in Fig. 2 as a function of the excited-lepton mass (m_{L^*}) for $f = f'$ and $f = -f'$. For charged excited leptons, the electromagnetic radiative

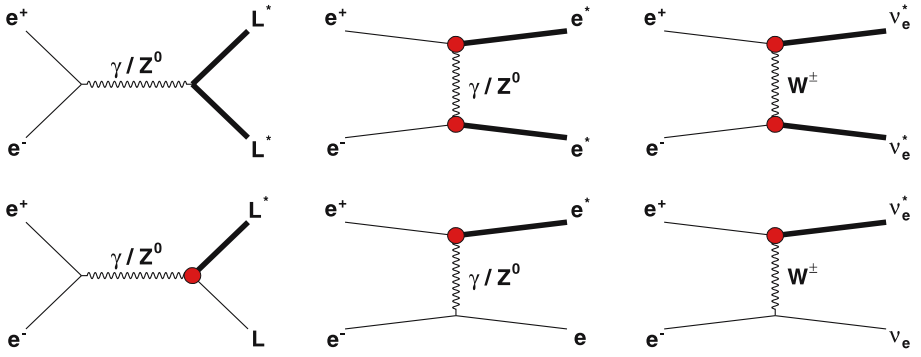

Fig. 1. Feynman diagrams for the double (*top*) and single (*bottom*) excited-lepton production. Each L^* is shown as a thicker line. The vertex shown as a *closed circle* represents a LL^*V coupling ($V \equiv \gamma, \mathrm{W}^{\pm}, \mathrm{Z}^0$) inversely proportional to the compositeness scale parameter Λ

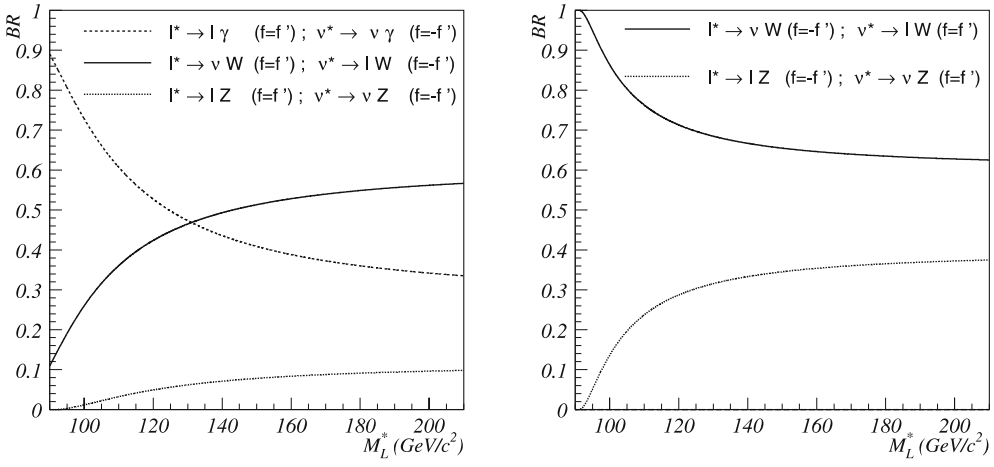

Fig. 2. Branching ratios of the excited-lepton decays as a function of the mass. In the *left plot* are shown the branching ratios for charged and neutral excited leptons when $f = f'$ and $f = -f'$, respectively. The *right plot* refers to the symmetric f and f' couplings assignment

decay is forbidden if $f = -f'$ and the decays proceed exclusively through Z^0 and $\mathrm{W}^{\pm}$ bosons. However, as long as $f \neq -f'$ there is a significant contribution to the total decay width from the electromagnetic radiative decay, even if $|f| - |f'| \ll |f|$. If $f = f'$, the electromagnetic radiative decay branching ratio is close to 100% for m_{L^*} smaller than the $\mathrm{W}^{\pm}$ mass (m_{W}), but decreases for $m_{L^*} > m_{\mathrm{W}}$ reaching a value of 34% for $m_{L^*} = 200$ GeV/c^2. For excited neutrinos the electromagnetic decays are forbidden only if $f = f'$.

Many final-state topologies arise from the production and decay of excited leptons. They involve isolated leptons, isolated photons, particle jets from quark fragmentation, missing energy ($\not\!\!E$) and missing momentum ($\not\!\!p$). Table 1 shows the topologies considered for the different L^* production and decay channels. Several of those, although not corresponding directly to the physical final state, are expected to become particularly important in presence of low energy or low polar angle[1] leptons.

The final states arising from the $\mathrm{W}^{\pm}$ or Z^0 leptonic decays in the single-production mode and the $\mathrm{W}^+\mathrm{W}^-$ purely leptonic decays or the $\mathrm{Z}^0\mathrm{Z}^0$ final states in the pair-production searches were not considered due to their small branching ratio and/or small signal sensitivity. In addition the pair-production search criteria aimed at selecting only the final state topologies where both excited leptons decay to identical gauge bosons (unmixed decays). Mixed decays where each excited lepton decays to a different gauge boson are not considered.

Table 1. Analysed final-state topologies corresponding to the different production and decay modes of excited leptons. The spectator or final state SM lepton remaining undetected is indicated by (ℓ)

Channel	Final-state Topologies	
	Single production	Pair production
$\ell^* \to \ell\gamma$	$\ell\ell\gamma$, $(\ell)\ell\gamma$	$\ell\ell\gamma\gamma$
$\ell^* \to \nu W$	$jj\ell\not\!\!E$, $jj(\ell)\not\!\!E$	$jj\ell\not\!\!E$, $jjjj\not\!\!E$
$\ell^* \to \ell Z$	$jj\ell\ell$, $jj\ell(\ell)$	–
$\nu^* \to \nu\gamma$	$\gamma\not\!\!E$	$\gamma\gamma\not\!\!E$
$\nu^* \to \ell W$	$jj\ell\not\!\!E$	$jj\ell\ell\ell$, $jj\ell\ell(\ell)$, $jjjj\ell\ell$
$\nu^* \to \nu Z$	$jj\not\!\!E$	–

3 Detector overview and data samples

The data analysed were collected with the DELPHI detector in the years 1998–2000, at centre-of-mass energies rang-

[1] In DELPHI a right-handed Cartesian coordinate system was used, with the z-axis pointing along the electron beam, the x-axis pointing toward the centre of the LEP ring and the origin at the centre of the detector. The polar angle θ is the angle to the electron beam direction and the azimuthal angle ϕ is the angle measured from the x-axis. In this paper θ also refers to the complementary angle $180^\circ - \theta$.

Table 2. Luminosity weighted mean centre-of-mass energy and integrated luminosities for the analysed data. The last column corresponds to the data taken after the TPC damage

Year	1998		1999			2000			
$\langle\sqrt{s}\,\rangle$ (GeV)	188.6	191.6	195.5	199.5	201.6	204.9	206.7	208.2	206.5
$\int \mathcal{L}$ (pb $^{-1}$)	151.8	25.1	76.0	82.6	40.1	79.9	77.1	6.9	59.2

ing from 189 GeV to 209 GeV and correspond to a total integrated luminosity of 598.7 pb^{-1}, with an average centre-of-mass energy of $\langle\sqrt{s}\,\rangle \simeq 198.5$ GeV. A detailed description of the DELPHI detector can be found in [9]. In the year 2000 the centre-of-mass energy varied from 201.5 GeV to 208.8 GeV, with an average value of $\langle\sqrt{s}\,\rangle \simeq 206$ GeV. With the purpose of maximizing the discovery potential, these data were subdivided into centre-of-mass energy bins that were analysed independently. During the year 2000 data taking an irrecoverable failure affected one sector of the central tracking detector (TPC), corresponding to 1/12 of its acceptance. The data recorded under these conditions, approximately 60 pb^{-1}, were analysed as an independent energy bin. The luminosity-weighted mean centre-of-mass energy and integrated luminosity for each analysed data set are summarised in Table 2. The last column corresponds to the data taken after the TPC damage. In the remainder of the text each centre-of-mass energy bin will be referred to by the nearest integer value and the energy bin corresponding to the data taken after the TPC failure as 206*. For the pair-production searches only the data taken in year 2000 were used in the analysis. In the single-production searches the 6.9 pb^{-1} collected at $\sqrt{s} \sim 208$ GeV were analysed together with the 207 GeV data.

Events from Standard Model processes contributing to the background were generated at each centre-of-mass energy using several Monte Carlo programs. $e^+e^- \to f\overline{f}(\gamma)$ events were generated with KK2F [10] (f= quark or muon), KORALZ [11] (f=tau) and BHWIDE [12] for Bhabha events (f=electron). Four-fermion final states were produced with WPHACT [13], while particular phase space regions of the $e^+e^- \to e^+e^-f\overline{f}$ process, referred to as two-photon interactions, were generated using PYTHIA [14] for hadronic final states, BDKRC [15] for $e^+e^-\mu^+\mu^-$ and $e^+e^-\tau^+\tau^-$ and BDK [16] for $e^+e^-e^+e^-$ final states. $e^+e^- \to e^+e^-\gamma$ events, with one electron (positron) scattered at very small polar angles while the positron (electron) and photon have large scattering angles, yield a final state with only one electron (positron) and one photon detected. Such events, which correspond to a particular region of the Bhabha scattering phase space not covered by the BHWIDE simulated sample, were generated according to [17]. The process $e^+e^- \to \gamma\gamma(\gamma)$ was simulated using the generator described in [18].

Excited-lepton events were simulated to study the distributions of the relevant kinematic variables and to compute the selection efficiencies of the analyses. Single- and pair-production events of all excited-lepton flavours were generated according to the differential cross-sections defined in [3]. Simulated events were produced at the relevant centre-of-mass energies and for several excited lepton masses. In the single-production scenario the following masses were considered at all centre-of-mass energies, m_{L^*} = 100, 125, 150, 170, 180 GeV/c^2; additional masses were produced up to the kinematic limit, with values depending on the centre-of-mass energy of the simulated sample (e.g. at $\sqrt{s} = 188.6$ GeV the masses 185 GeV/c^2 and 188 GeV/c^2 were also simulated). In the pair production the following masses were simulated: m_{L^*} = 85, 90, 95, 100 and 103 GeV/c^2. In addition, for $\ell^*\ell^* \to \nu\mathrm{W}\nu\mathrm{W}$ the m_{L^*} values between 95 and 103 GeV/c^2 were taken in 1 GeV/c^2 steps.

In all simulations the relation $f = f'$ was assumed. However, in the case of the single production of excited electrons, events were generated also with $f = -f'$. This allowed to take into account the strong dependence of the event kinematics on the relative weights of the couplings. In the single-production mode, initial-state radiation (ISR) of photons was included at the event generation level, while for the pair-production process it was taken into account in the computation of the total cross-section.

All excited-lepton decay modes were included in the single-production simulations. For the pair production the following unmixed decays were simulated: $\ell^*\ell^* \to \ell\ell\gamma\gamma$, $\nu^*\nu^* \to \nu\nu\gamma\gamma$, $\ell^*\ell^* \to \nu\mathrm{W}\nu\mathrm{W}$ and $\nu^*\nu^* \to \ell\mathrm{W}\ell\mathrm{W}$. Finally the decays of $\mathrm{W}^\pm$ and Z^0 bosons and tau leptons and the hadronization/fragmentation in hadronic final states were performed using JETSET 7.4 [14].

The generated signal and background events were passed through the detailed simulation of the DELPHI detector and then processed with the same reconstruction and analysis programs as the real data [9]. For the data collected after the TPC failure the reconstruction software for charged particle tracks was adjusted to make best use of the Silicon Tracker and Inner Detector, both placed closer to the beam than the TPC, and the Outer Detector and Barrel Rich, placed outside the TPC. As a result, the impact of the malfunctioning TPC sector on the determination of jet momenta was not large. A dedicated simulation of the detector conditions during this period was also used.

4 Event selection

The production and decay of excited leptons would yield topologies involving isolated leptons, isolated photons, jets and missing energy, as detailed in Table 1.

In the first step of the analysis, isolated photons and charged leptons are searched by constructing double cones

centred in the direction of the charged particle tracks and the neutral energy deposits, defined as energy deposits in the calorimeters not matched to charged particle tracks. The energy detected inside an inner cone with half opening angle of 5° must be greater than 5 GeV, while the energy contained between the inner cone and the outer cone must be small to ensure isolation. Both the opening angle of the outer cone and the maximal accepted total energy contained between the two cones can vary as detailed in [19].

Events are pre-selected by requiring the total energy deposited above 20° in polar angle to be greater than $0.2\sqrt{s}$. The events are then classified in different topologies according to their multiplicity and to the number of isolated leptons and photons. The "low-multiplicity" events contain at most five well-reconstructed tracks while "high-multiplicity" events have more than five such tracks. In "low-multiplicity" events all particles not identified as isolated photons are clustered into jets using the Durham algorithm [20]. This allows to handle the decay products of the tau leptons as low-multiplicity jets. The jets in the event are obtained by requiring the jet resolution variable to be greater than 0.003 for all jet pairings [6]. If the number of jets thus obtained is smaller than the number of isolated leptons previously found, the algorithm is applied once more requiring the number of jets to be equal to the number of isolated leptons. For the "high-multiplicity" events no dedicated strategy for the taus was followed. In this case a tau is reconstructed only if its decay products (charged leptons or low-multiplicity jets) fulfil the double cone isolation criteria. Electron, photon and muon identification are based on the standard DELPHI algorithms described in [9]. Topology-dependent criteria are finally applied, as detailed in the following subsections, and, whenever possible, the flavour of the final-state leptons is used to tag the flavour of the excited lepton.

4.1 Topologies with only photons

Final-state topologies consisting of photons only could arise from the production of excited neutrinos decaying to a SM neutrino and a photon. For these topologies the analyses presented in [19] and [21] were used.

In the search for single production of excited neutrinos, events consisting of only one photon in DELPHI (single-photon events) are considered. For the single-photon preselection the results from [21] were used. The background from SM processes giving single-photon events is mainly due to the process $e^+e^- \to \mathrm{Z}^0\gamma \to \nu\overline{\nu}\gamma$, where the final-state photon is emitted predominantly at small polar angles. Candidate events must have a photon with polar angle $\theta_\gamma > 45°$ and with energy $E_\gamma > 0.45\sqrt{s}$. In the $\nu\nu^*$ search the data from year 2000 was grouped in two bins, corresponding to $\sqrt{s} < 207$ GeV (including the 206* data) and $\sqrt{s} \geq 207$ GeV.

For the $\nu^*\nu^*$ search events with two photons were selected. The selection of events with two photons and missing energy described in [19] was followed, except for the kinematic fit imposing the Z^0 mass on the invisible system and the requirement on the missing mass.

4.2 Topologies with leptons and photons

Topologies with isolated leptons and photons are expected whenever the excited charged leptons decay by photon emission.

For the single-production search the topologies $\ell\ell\gamma$ and $\ell\gamma$ were considered as shown in Table 1. The $\ell\gamma$ topology becomes dominant for all flavours when the excited-lepton mass is close to the centre-of-mass energy. The spectator SM lepton has then too small an energy to be identified as an isolated particle. The $\ell\gamma$ topology is also crucial for the single e^* search when t-channel production dominates, in particular for the $f = f'$ scenario. The SM spectator electron is then scattered at small polar angles, remaining undetected.

Different preselection criteria were applied, according to the event classification in each of the topologies and taking into account the relevant background processes and the specific kinematics of the signal events.

Only events with at least one photon with energy $E_\gamma > 0.05\sqrt{s}$ are considered; for the lepton momentum (p_ℓ) it is required $p_\ell > 0.05\sqrt{s}$ in the topologies with only one lepton. In the $\ell\ell\gamma$ topology the sum of the two lepton momenta must be greater than $0.1\sqrt{s}$. The sum of the lepton and photon energies ($p_{\ell_1} + p_{\ell_2} + E_\gamma$) should in principle be of the order of the centre-of-mass energy; however, since in $\tau\tau^* \to \tau\tau\gamma$ events a fraction of the energy is carried by neutrinos, it is required $p_{\ell_1} + p_{\ell_2} + E_\gamma > 0.4\sqrt{s}$. In the e^* and μ^* searches, the momentum of the most energetic lepton must be greater than $0.05\sqrt{s}$. For events in the $\ell\gamma$ topology it is required that $E_\gamma > 0.1\sqrt{s}$, $p_\ell > 0.1\sqrt{s}$ and $E_\gamma + p_\ell > 0.4\sqrt{s}$.

Figure 3 shows the distribution, after this preselection, of relevant kinematic variables for each of the topologies considered.

The event selection was further tightened as follows. In the case of the $\ell\gamma$ topology the dominant background arise from Bhabha scattering events with one electron lost at low polar angle or identified as a photon. Requiring the presence of an energetic photon in the central region of the detector is the main rejection criterium. For the e^* and τ^* searches in this topology it is thus required that $\theta_\gamma > 42°$.

The main background for the $\ell\ell\gamma$ topology is due to radiative Bhabha scattering events. Initial-state radiation events, where the photon is mainly emitted at small polar angle, are reduced by requiring $\theta_\gamma > 42°$ in the e^* and τ^* searches. The background from final-state radiation consists of low-energy photons emitted at small angle to the direction of the final-state leptons. It is thus required $E_\gamma \cdot \sin\alpha > 0.08\sqrt{s}$, where E_γ is the photon energy and α is the angle between the photon direction and the direction of the nearest particle.

The final-state topology consisting of one electron and two photons, $e\gamma\gamma$, was additionaly considered in the e^* search. In the t-channel-dominated e^* production mode the spectator electron scattered in the forward direction could be detected by the low-angle calorimeter of DELPHI, below the geometrical acceptance of the tracking detectors, thus being reconstructed as a photon. For the selection of events in the $e\gamma\gamma$ topology only one photon with $\theta_\gamma < 9°$

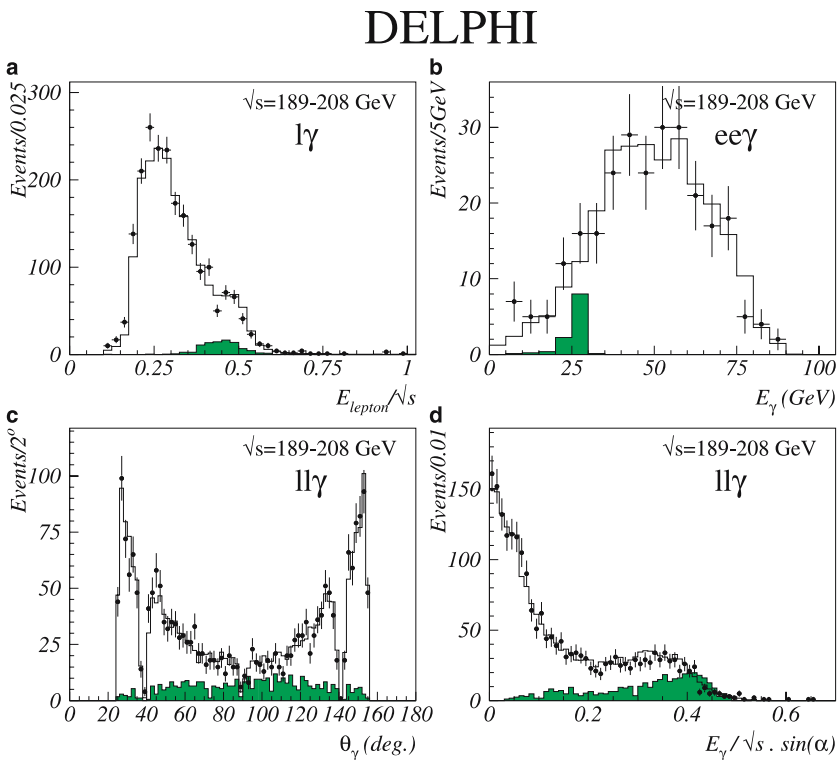

Fig. 3. Topologies with leptons and photons after the preselection cuts: **a** lepton energy in the $\ell\gamma$ topology; **b** energy of the least energetic photon in the e* search in the final-state topology with one electron and two reconstructed photons; **c** photon polar angle and **d** $E_\gamma/\sqrt{s}\cdot\sin\alpha$, where α is the minimum angle between the photon direction and the two lepton directions, in the $\ell\ell\gamma$ topology. The *dots* show the data and the *white histograms* show the SM simulation. The *shaded histograms* show the expected distributions for a $m_{L^*} = 175\,\mathrm{GeV}/c^2$ excited lepton at $\sqrt{s} = 206\,\mathrm{GeV}$, using an arbitrary normalization

can be present; the other photon must be detected above 25°; the sum of the lepton momentum and photon energies is above $0.8\sqrt{s}$. The main background for this topology is due to radiative Bhabha scattering events, with one low angle electron being identified as a photon. This background is mostly irreducible. Some reduction of the background is achieved by requiring that $p_\ell + E_{\gamma_1} > 0.4\sqrt{s}$, where E_{γ_1} is the energy of the low polar-angle photon.

For the pair-production searches the $\ell\ell\gamma\gamma$ topology was considered. The expected background is rather low and simpler cuts were applied. Both leptons must have momentum above $10\,\mathrm{GeV}/c$. Events are kept as candidates if a lepton-photon pairing exists for which the difference between the invariant masses of the two lepton-photon pairs is smaller than $15\,\mathrm{GeV}/c^2$ ($20\,\mathrm{GeV}/c^2$) in the e^* and μ^* (τ^*) searches.

The excited-lepton mass can be reconstructed by computing the lepton-photon invariant mass. In the $e\gamma\gamma$ topology the photon expected from the decay of an excited electron is the one detected at high polar angle, while in the $\ell\ell\gamma$ topology both possible lepton-photon pairings are considered. The invariant-mass resolution improves by rescaling the measured energies and momenta. This is done imposing energy-momentum conservation and using just the polar and azimuthal angles, which are well measured in the detector. Resolution of ±1 mrad in θ and ±1.7 mrad in ϕ are obtained for high energy photons and of about ±1 mrad or better in θ and ϕ are obtained for high momentum charged particle tracks, in the central part of the DELPHI detector [9]. In order to take into account the energy lost through initial-state radiation, the rescaling is also applied assuming the presence of an additional photon along the beam direction. This procedure accounts also for the case when the spectator electron is lost in the beam pipe. The compatibility of the rescaled and the measured values is quantified through the χ^2 parameter [5, 6]. The χ^2 was computed separately for charged particles ($\chi^2_{\mathrm{charged}}$) and photons ($\chi^2_{\mathrm{photons}}$). The result from the rescaling assuming an additional particle along the beam direction was retained whenever it yielded a smaller total χ^2. In any case only events with $\min(\chi^2_{\mathrm{charged}}, \chi^2_{\mathrm{photons}}) < 5$ are retained. The resolution on the lepton-photon invariant mass, after applying the kinematic constraints, is in the range $0.2-0.6\,\mathrm{GeV}/c^2$ ($1.5-2.0\,\mathrm{GeV}/c^2$) for electrons and muons (taus).

Finally, the flavour of the final-state leptons is used to select the candidate events. In the e^* search all leptons must be identified as electrons. The search for μ^* requires that the most energetic lepton is identified as a muon and no particle is identified as an electron. In the τ^* search no lepton flavour identification is applied; instead, a difference between the measured and rescaled momenta of the final-state leptons, characteristic of the presence of neutrinos from tau decays, is required by imposing $\chi^2_{\mathrm{charged}} > 5$ in the single-production and $\chi^2_{\mathrm{charged}} > 10$ in the pair-production searches.

4.3 Topologies with jets and leptons

Final-state topologies with jets and isolated leptons were considered in the search for excited leptons decaying to $\mathrm{W}^\pm$ or Z^0, $\ell^* \to \nu\mathrm{W}$, $\ell^* \to \ell\mathrm{Z}^0$, $\nu^* \to \ell\mathrm{W}$ and $\nu^* \to \nu\mathrm{Z}^0$. Due to the presence of neutrinos, some of the topologies are additionaly characterized by missing energy. In the single-production searches only the final states arising from the

hadronic decays of the $W^{\pm}$ and Z^0 bosons were addressed. In the pair-production searches only the fully hadronic or semileptonic decays of the W^+W^- pairs were addressed. The "high-multiplicity" events were thus considered in these analyses.

4.3.1 Single-production analysis

The topologies considered in the single-production search are $jj\not{E}$, $jj\ell\not{E}$, $jj\ell$ and $jj\ell\ell$. All particles in the event, excluding the isolated leptons, are clustered into jets using the Durham algorithm. Two-jet events are selected by requiring the Durham jet resolution variable for the transition from three to two jets, y_{23}, to be lower than 0.06 and from two to one jet, y_{12}, to be greater than 0.01. The polar angle of isolated leptons must be above 25°.

The searches for pair production of excited leptons already excluded L^* masses smaller than the mass of the Z^0 boson for all excited lepton flavours. The gauge bosons are thus expected to be produced on-shell and the invariant mass of the two jets (M_{jj}) should be compatible with a $W^{\pm}$ or Z^0 boson. The loose condition $40 < M_{jj} < 120\ \mathrm{GeV}/c^2$ is thus applied in all topologies. In addition, since the gauge bosons originating from excited-lepton decays are not at rest, the two jets are also expected to be acoplanar. This characteristic is quantified by the jet-jet acoplanarity, A^{jj}_{cop}, defined as $180° - \Phi$, where Φ is the angle between the projections of the jet momenta in the plane perpendicular to the beam.

For events in the jj topology the main background comes from $e^+e^- \to q\overline{q}(\gamma)$ events, where the photon is emitted at a very small polar angle or is soft, and thus remains undetected. Since the transverse momentum of the photon is always very small (typically $< 2\ \mathrm{GeV}/c$ at $\sqrt{s} = 200$ GeV), this process results in two jets with small acoplanarity. Candidate events are required to have $A^{jj}_{\mathrm{cop}} > 25°$ and the polar angle of both jets larger than 20°.

A looser acoplanarity cut, $A^{jj}_{\mathrm{cop}} > 10°$, is applied to events in the $jj\ell$ topology. The background is mainly due to W^+W^- production, with one boson decaying to quarks and the other to a charged lepton and a neutrino ($W^{\pm}$ semileptonic decays). The quantity $\xi = Q_W \cdot cos\theta_W$, Q_W and θ_W being the boson charge and polar angle respectively, was used to reduce the W^+W^- background. The $W^{\pm}$ bosons in background events are produced preferentially in the forward direction and ξ is peaked towards -1. In $W^{\pm}$ semileptonic decays Q_W is given by the lepton charge and θ_W is estimated, neglecting radiation effects, from the jet directions. For events in the $jj\ell$ topology with the lepton charge unambiguously determined, about 90% of the events, it is required $\xi > -0.6$, while no condition is applied to the remaining events.

In the $jj\ell\ell$ topology the angle between the two lepton directions or between any of the leptons and the jet directions must be greater than 10°. No acoplanarity cut is applied.

Figure 4 shows the distributions for the jet-jet acoplanarity, the variable ξ for events with the lepton charge unambiguously determined and the energy of the most energetic lepton, for the jj, $jj\ell$ and $jj\ell\ell$ topologies, after the preselection cuts.

In order to improve the estimation of the jet momenta and energies a kinematic fit [22] is applied to the selected events. Events in the jj and $jj\ell$ topologies can arise from excited-lepton decays mediated by a $W^{\pm}$ or Z^0 boson and thus the invariant mass of the jet-jet system is constrained

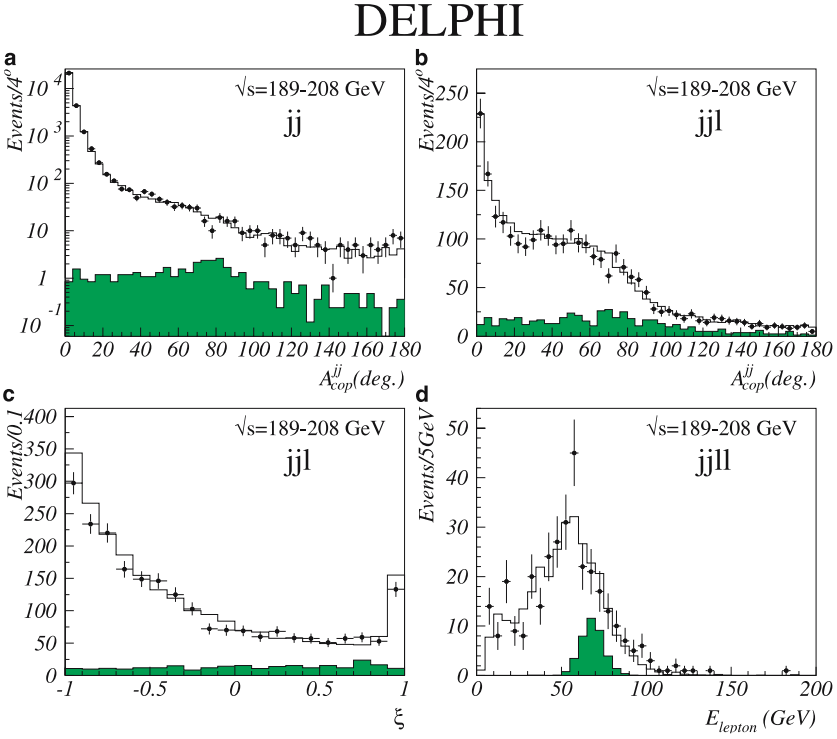

Fig. 4. Topologies with jets and leptons after the preselection cuts: **a** jet-jet acoplanarity in the jj topology; **b** jet-jet acoplanarity in the $jj\ell$ topology; **c** variable $\xi = Q_W \cdot \cos\theta_W$ in the $jj\ell$ topology, for events with the lepton charge unambiguously determined; **d** energy of the most energetic lepton in $jj\ell\ell$ events. The *dots* show the data and the *white histograms* show the SM simulation. The *shaded histograms* show the expected distributions for a $m_{L^*} = 175\ \mathrm{GeV}/c^2$ excited lepton at $\sqrt{s} = 206$ GeV, using an arbitrary normalization

to be either m_W or m_Z, depending on the search channel. For events in the $jj\ell\ell$ topology only the m_Z constraint is used. In all cases, only the events compatible with the expected decay mode are retained by requiring that the kinematic fit yielded a χ^2 per degree of freedom lower than 5.

The excited-lepton mass can be estimated in several of the topologies considered. The relevant variables are the jet-jet-lepton ($\nu\nu^* \to \nu\ell\mathrm{W}^\pm$) and jet-jet-neutrino ($\ell\ell^* \to \ell\nu\mathrm{W}^\pm$) invariant masses, and the recoil mass of isolated leptons ($\ell\ell^* \to \ell\nu\mathrm{W}^\pm$, $\ell\ell^* \to \ell\ell\mathrm{Z}^0$). The neutrino four momenta (P_ν) was reconstructed, from the total energy (E) and momenta ($\overrightarrow{p}$) of all measured final-state particles, as $P_\nu = (\overrightarrow{0}, \sqrt{s}) - (\overrightarrow{p}, E)$. The resolution on the jet-jet-neutrino invariant mass varies between $1\,\mathrm{GeV}/c^2$ and $5\,\mathrm{GeV}/c^2$. In the $\tau\tau^* \to \tau\nu\mathrm{W}^\pm$ channel, the τ^* mass is reconstructed only for signal masses $m_{\tau^*} > 0.9\sqrt{s}$ and is obtained from the recoil mass of the spectator lepton; the resolution ranges between $3\,\mathrm{GeV}/c^2$ and $6\,\mathrm{GeV}/c^2$. The resolution on the jet-jet-lepton invariant mass is about $2\,\mathrm{GeV}/c^2$ for $m_{\nu^*} = 100\,\mathrm{GeV}/c^2$, increasing to about $10\,\mathrm{GeV}/c^2$ for $m_{\nu^*} = 200\,\mathrm{GeV}/c^2$; no mass reconstruction was attempted in the ν_τ^* channel.

At the last step of the analysis, the various production and decay modes within the same topology are treated differently. In the searches for excited leptons of the first and second generations, the flavour of the final-state isolated leptons must match the excited-lepton flavour. In the searches for τ^* and ν_τ^* in the topologies with isolated leptons no selection is applied based on the flavour of the final-state leptons. Instead, due to the presence of neutrinos in the tau decay products, the final-state isolated leptons are expected to have relatively small energy. Therefore a cut on the energy of the final-state leptons is used as follows: in the $\tau^* \to \tau\mathrm{Z}^0$ search, the energy of the isolated lepton must be lower than $0.3\sqrt{s}$ for events in the $jj\ell$ topology, while in the $jj\ell\ell$ topology at least one lepton with energy smaller than $0.2\sqrt{s}$ must be present; in the $\nu_\tau^* \to \tau\mathrm{W}^\pm$ search the lepton energy must be smaller than $0.2\sqrt{s}$.

4.3.2 Pair-production analysis

$\nu^*\nu^*$ search. In the search for pair production of neutral excited leptons decaying to $\mathrm{W}^\pm$ bosons ($\nu^*\nu^* \to \ell\mathrm{W}\ell\mathrm{W}$) only the fully hadronic and semileptonic decays of $\mathrm{W}^+\mathrm{W}^-$ pairs were taken into account. The final-state topologies are formed by the $\mathrm{W}^+\mathrm{W}^-$ decay products (two jets and one lepton or four jets) and by two additional charged leptons, yielding a rather clear signature.

Multijet events are selected by requiring $y_{12} > 0.03$ and only events with at least two isolated leptons are kept. If exactly two isolated leptons are found it is further required that $y_{23} > 0.01$.

In the search for ν_e^* and ν_μ^* , the final state must contain at least two charged leptons of the corresponding flavour. For the ν_τ^* search it is required $\not\!\!E > 0.1\sqrt{s}$.

$\ell^*\ell^*$ search. The final-state topologies considered in the search for pair production of charged excited leptons decaying to $\mathrm{W}^\pm$ bosons ($\ell^*\ell^* \to \nu\mathrm{W}\nu\mathrm{W}$) were four jets or two jets and one lepton. They result respectively from the fully hadronic or semileptonic decays of the $\mathrm{W}^+\mathrm{W}^-$ pair.

Contrary to the $\nu^*\nu^*$ search described above, the two additional particles in the final state are now neutrinos, giving missing energy. Signal events have thus a signature very similar to the $\mathrm{W}^+\mathrm{W}^-$ background events. A discriminant analysis was used in the $\ell^*\ell^* \to \nu\mathrm{W}\nu\mathrm{W}$ search, in order to boost the small differences between the signal and background kinematics. After the event preselection a signal likelihood, $\mathcal{L}_S$, and a background likelihood, $\mathcal{L}_B$, are constructed as the product of probability density functions (PDFs) of relevant kinematic variables, as described below. The discriminant variable is defined as $\mathcal{L}_S/\mathcal{L}_B$.

The semileptonic and the fully hadronic cases were treated separately. In the semileptonic analysis only events with no isolated photons and at least one isolated lepton are considered. The remaining particles in the event are clustered into jets. Two-jet events are selected by requiring $y_{23} < 0.06$ and $y_{12} > 0.01$. The background from $e^+e^- \to q\overline{q}(\gamma)$ events is reduced by requiring the polar angle of the direction of the missing momentum to be above 20°. The minimum transverse momentum of the lepton with respect to any of the jets must be greater than $10\,\mathrm{GeV}/c$; the lepton polar angle is required to be above 20° for muons and above 40° for electrons. The following variables are then used to build the discriminant variable:

- the missing energy of the event;
- the angle between the two jets;
- the energy of the lepton;
- the angle between the lepton and missing momentum directions;
- the $\mathrm{Q}_\ell \cdot \cos\theta_\ell$ variable, where Q_ℓ and θ_ℓ are the charge and polar angle of the lepton.

In the fully hadronic analysis it is required that no isolated photons or leptons are found. Four-jet events are selected by requiring $y_{34} > 0.003$ and $y_{23} > 0.03$. The jets are assigned to each of the $\mathrm{W}^\pm$ bosons by choosing the pairing that minimizes the sum of the squares of the differences between the jet-jet invariant masses and the $\mathrm{W}^\pm$ mass. A fit imposing energy-momentum conservation and constraining the invariant mass of the two jet pairs to the $\mathrm{W}^\pm$ mass is performed. The following quantities are then used to build the discriminant variable:

- the missing energy of the event;
- the angle between the directions of the two jets of each pair;
- the angle between the two reconstructed W bosons.

The distributions of some of the variables used to build $\mathcal{L}_S/\mathcal{L}_B$ are shown in Fig. 5. A good agreement with the SM predictions is observed. It should be noted that due to the finite resolution in the measurement of the charged particle tracks and calorimeter energy deposits, the missing energy of the event $\not\!\!E = \sqrt{s} - E_{\mathrm{vis}}$, with E_{vis} the total measured energy in the event, may fluctuate to negative values.

In Fig. 6 are shown the distributions of $\mathcal{L}_S/\mathcal{L}_B$ for the semileptonic and the hadronic final states.

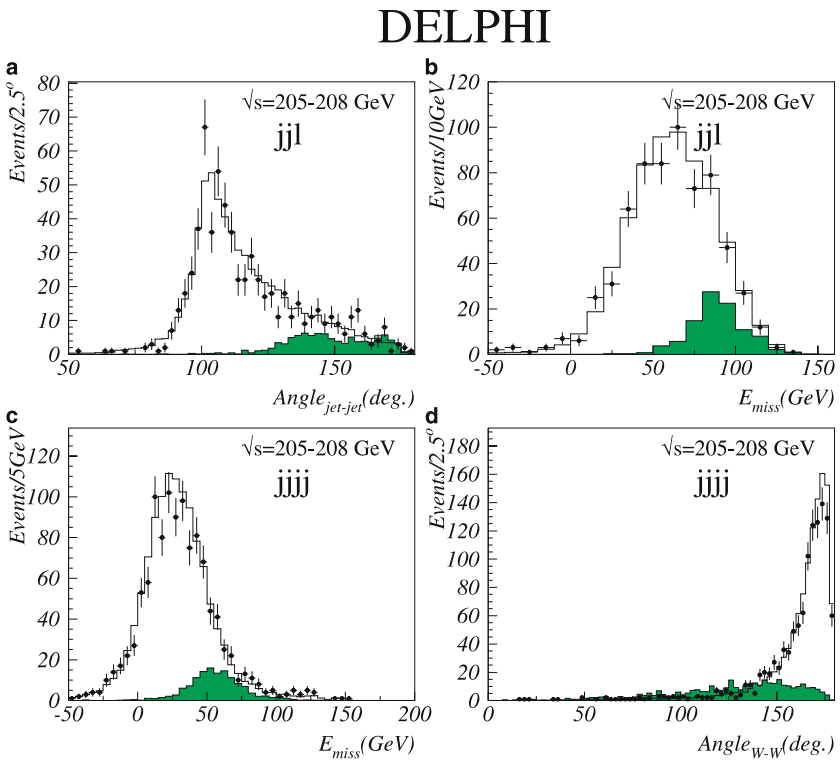

Fig. 5. $\ell^*\ell^*$ search at the preselection level: **a** angle between the two jets and **b** missing energy in the semileptonic channel; **c** missing energy and **d** angle between the two reconstructed Ws in the fully hadronic channel. The *dots* show the data and the *white histograms* show the expected SM background. The *shaded histograms* show the expected signal distributions at $\sqrt{s} = 206$ GeV with m_{L^*}=100 GeV/c^2, using an arbitrary normalization

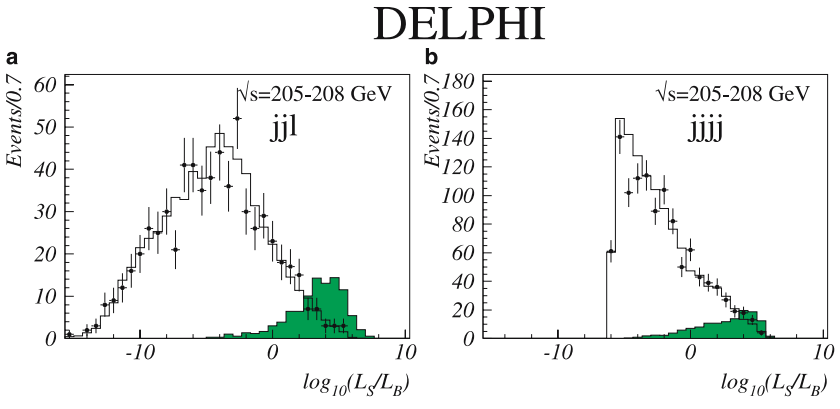

Fig. 6. $\ell^*\ell^*$ search: discriminant variables in the **a** semileptonic and **b** fully hadronic channels. The *dots* are the data and the *white histograms* show the SM background expectation. The *shaded histograms* are the expected distributions for a $m_{L^*} = 100$ GeV/c^2 signal at $\sqrt{s} = 206$ GeV, using an arbitrary normalization

5 Results

No evidence for the production of excited leptons was observed in any of the final states considered. The number of candidate events found at the various centre-of-mass energies, together with the expected background from SM processes, are summarized in Tables 3 and 4, for the different excited-lepton flavours and decay modes. The total numbers are summarized in Table 5. These numbers are obtained by adding the results from the different exclusive final state topologies considered in each decay (as listed in Table 1). The relevance of each topology depends on the decay branching ratios, which are a function of the excited-lepton mass and of the coupling parameters. In many cases there are candidate events common to the different excited-lepton searches (e.g. the events selected in the jj topology are candidates in all $\ell^* \to \nu W$ searches, independent of the ℓ^* flavour), but in the search for a given flavour there are no common candidates selected in final states originating from different decay modes.

The signal selection efficiencies at $\sqrt{s} = 206$ GeV are given in Table 6, for specific values of m_{L^*}. In most of the channels the dependence of the efficiency on the mass is weak, as we benefited from the combination of results from several final-state topologies which are sensitive to different mass regions.

Figures 7 and 8 show the invariant mass distributions for the candidates selected in the various single-production searches, obtained by adding the data from all the analysed centre-of-mass energies and topologies.

5.1 Systematic uncertainties

Systematic uncertainties affect both the background and the signal efficiency estimations.

Table 3. Number of candidates for the different excited-lepton decay channels in the single-production search. The numbers in parentheses correspond to the SM background expectations with the statistical errors

$\sqrt{s}$		Excited-lepton flavour					
(GeV)	Channel	e		μ		τ	
	$\ell^* \to \ell\gamma$	366	(408.2 ± 6.7)	39	(44.0 ± 1.5)	62	(54.3 ± 2.7)
	$\ell^* \to \nu W^\pm$	202	(217.6 ± 4.8)	195	(195.5 ± 4.3)	432	(447.8 ± 7.1)
189	$\ell^* \to \ell Z^0$	51	(42.0 ± 3.4)	8	(10.00 ± 0.66)	55	(40.9 ± 2.7)
	$\nu^* \to \nu\gamma$			3	(0.70 ± 0.17)		
	$\nu^* \to \ell W^\pm$	175	(180.1 ± 4.9)	133	(131.3 ± 3.2)	203	(196.5 ± 4.9)
	$\nu^* \to \nu Z^0$			75	(81.1 ± 3.1)		
	$\ell^* \to \ell\gamma$	61	(66.4 ± 2.0)	8	(7.29 ± 0.27)	10	(8.05 ± 0.76)
	$\ell^* \to \nu W^\pm$	28	(38.04 ± 0.79)	25	(33.71 ± 0.69)	56	(75.2 ± 1.1)
192	$\ell^* \to \ell Z^0$	5	(5.24 ± 0.44)	1	(2.01 ± 0.16)	3	(6.56 ± 0.43)
	$\nu^* \to \nu\gamma$			0	(0.10 ± 0.03)		
	$\nu^* \to \ell W^\pm$	24	(28.53 ± 0.75)	18	(22.01 ± 0.53)	26	(31.33 ± 0.79)
	$\nu^* \to \nu Z^0$			9	(14.87 ± 0.49)		
	$\ell^* \to \ell\gamma$	201	(188.9 ± 3.3)	18	(20.27 ± 0.73)	24	(23.4 ± 1.3)
	$\ell^* \to \nu W^\pm$	108	(117.3 ± 2.4)	103	(101.6 ± 2.1)	232	(230.0 ± 3.5)
196	$\ell^* \to \ell Z^0$	26	(20.4 ± 1.5)	3	(5.81 ± 0.36)	23	(21.0 ± 1.2)
	$\nu^* \to \nu\gamma$			2	(0.70 ± 0.08)		
	$\nu^* \to \ell W^\pm$	90	(91.2 ± 2.3)	72	(64.6 ± 1.6)	106	(96.7 ± 2.4)
	$\nu^* \to \nu Z^0$			38	(45.6 ± 1.5)		
	$\ell^* \to \ell\gamma$	190	(198.8 ± 3.5)	25	(20.74 ± 0.74)	26	(27.3 ± 1.3)
	$\ell^* \to \nu W^\pm$	128	(131.1 ± 2.6)	102	(114.6 ± 2.4)	239	(248.0 ± 3.7)
200	$\ell^* \to \ell Z^0$	29	(19.3 ± 1.4)	9	(7.05 ± 0.48)	28	(22.4 ± 1.3)
	$\nu^* \to \nu\gamma$			6	(1.7 ± 0.1)		
	$\nu^* \to \ell W^\pm$	116	(96.7 ± 2.4)	70	(70.5 ± 1.7)	108	(102.5 ± 2.5)
	$\nu^* \to \nu Z^0$			42	(52.2 ± 1.7)		
	$\ell^* \to \ell\gamma$	87	(94.9 ± 2.1)	8	(9.44 ± 0.38)	16	(12.05 ± 0.73)
	$\ell^* \to \nu W^\pm$	79	(61.9 ± 1.2)	54	(54.1 ± 1.1)	138	(119.6 ± 1.8)
202	$\ell^* \to \ell Z^0$	5	(10.53 ± 0.77)	4	(3.45 ± 0.25)	9	(11.42 ± 0.68)
	$\nu^* \to \nu\gamma$			1	(1.2 ± 0.1)		
	$\nu^* \to \ell W^\pm$	54	(46.8 ± 1.2)	28	(33.57 ± 0.84)	55	(51.4 ± 1.3)
	$\nu^* \to \nu Z^0$			31	(24.91 ± 0.80)		
	$\ell^* \to \ell\gamma$	179	(182.7 ± 3.8)	20	(18.28 ± 0.34)	27	(24.3 ± 1.2)
	$\ell^* \to \nu W^\pm$	119	(123.8 ± 2.4)	94	(102.4 ± 2.1)	225	(231.5 ± 3.4)
205	$\ell^* \to \ell Z^0$	22	(18.0 ± 1.3)	7	(6.82 ± 0.47)	24	(21.5 ± 1.3)
	$\nu^* \to \nu\gamma$			5	(1.3 ± 0.2)		
	$\nu^* \to \ell W^\pm$	98	(90.9 ± 2.3)	60	(61.8 ± 1.6)	88	(100.1 ± 2.4)
	$\nu^* \to \nu Z^0$			46	(50.5 ± 1.6)		
	$\ell^* \to \ell\gamma$	120	(129.8 ± 2.7)	11	(13.15 ± 0.25)	16	(19.2 ± 1.0)
	$\ell^* \to \nu W^\pm$	79	(93.9 ± 1.8)	70	(79.8 ± 1.7)	138	(173.1 ± 2.5)
206*	$\ell^* \to \ell Z^0$	15	(14.3 ± 1.0)	3	(4.51 ± 0.35)	16	(14.75 ± 0.88)
	$\nu^* \to \ell W^\pm$	58	(67.4 ± 1.7)	41	(46.4 ± 1.2)	53	(72.3 ± 1.7)
	$\nu^* \to \nu Z^0$			37	(38.9 ± 1.2)		
> 206	$\nu^* \to \nu\gamma$			1	(2.6 ± 0.2)		
	$\ell^* \to \ell\gamma$	172	(180.9 ± 3.3)	15	(18.28 ± 0.34)	21	(25.1 ± 1.2)
	$\ell^* \to \nu W^\pm$	110	(130.6 ± 2.5)	94	(110.7 ± 2.3)	205	(239.3 ± 3.5)
207	$\ell^* \to \ell Z^0$	30	(22.8 ± 1.6)	6	(6.9 ± 0.5)	21	(23.4 ± 1.3)
+	$\nu^* \to \ell W^\pm$	86	(96.4 ± 2.4)	52	(64.9 ± 1.7)	87	(99.9 ± 2.4)
208	$\nu^* \to \nu Z^0$			53	(55.3 ± 1.7)		

Table 4. Number of excited-lepton candidates for the different decay channels and centre-of-mass energies in the pair-production search. The numbers in parentheses correspond to the SM background expectations with the statistical errors

$\sqrt{s}$ (GeV)	Channel	Excited-lepton flavour e		μ		τ	
	$\ell^* \to \ell\gamma$	0	(1.25 ± 0.33)	0	(0.38 ± 0.05)	1	(2.57 ± 0.41)
	$\ell^* \to \nu W$ (hadr.)			403	(419.9 ± 5.1)		
	$\ell^* \to \nu W$ (semilep.)			261	(231.1 ± 3.1)		
205	$\nu^* \to \nu\gamma$			4	(3.26 ± 0.33)		
	$\nu^* \to \ell W$	1	(3.21 ± 0.33)	1	(0.99 ± 0.16)	18	(17.43 ± 0.87)
	$\ell^* \to \ell\gamma$	1	(0.52 ± 0.20)	0	(0.29 ± 0.04)	3	(1.48 ± 0.27)
	$\ell^* \to \nu W$ (hadr.)			280	(311.0 ± 3.8)		
	$\ell^* \to \nu W$ (semilep.)			154	(176.6 ± 2.4)		
206*	$\nu^* \to \nu\gamma$			6	(2.21 ± 0.26)		
	$\nu^* \to \ell W$	6	(2.56 ± 0.32)	0	(0.93 ± 0.14)	15	(12.04 ± 0.61)
	$\ell^* \to \ell\gamma$	1	(1.49 ± 0.34)	2	(0.41 ± 0.05)	3	(2.59 ± 0.39)
	$\ell^* \to \nu W$ (hadr.)			408	(416.9 ± 5.0)		
	$\ell^* \to \nu W$ (semilep.)			228	(239.0 ± 3.2)		
207	$\nu^* \to \nu\gamma$			3	(3.50 ± 0.36)		
	$\nu^* \to \ell W$	3	(3.10 ± 0.32)	1	(1.74 ± 0.22)	20	(17.22 ± 0.89)
	$\ell^* \to \ell\gamma$	0	(0.16 ± 0.06)	0	(0.04 ± 0.01)	0	(0.25 ± 0.07)
	$\ell^* \to \nu W$ (hadr.)			34	(34.95 ± 0.85)		
	$\ell^* \to \nu W$ (semilep.)			10	(19.94 ± 0.54)		
208	$\nu^* \to \nu\gamma$			–			
	$\nu^* \to \ell W$	0	(0.36 ± 0.08)	0	(0.10 ± 0.02)	2	(1.68 ± 0.17)

Table 5. Total number of candidates for the different excited lepton decay channels in the single (*top*) and pair (*bottom*) production searches. The numbers in parentheses correspond to the SM background expectations with the statistical errors

Channel	Excited-lepton flavour e		μ		τ	
			Single production			
$\ell^* \to \ell\gamma$	1376	(1451 ± 10)	144	(151.5 ± 2.0)	202	(193.7 ± 4.0)
$\ell^* \to \nu \mathrm{W}^\pm$	853	(914.2 ± 7.3)	737	(792.4 ± 6.5)	1665	(1765 ± 11)
$\ell^* \to \ell \mathrm{Z}^0$	183	(152.6 ± 4.7)	41	(46.5 ± 1.2)	179	(161.9 ± 3.9)
$\nu^* \to \nu\gamma$			18	(8.3 ± 0.4)		
$\nu^* \to \ell \mathrm{W}^\pm$	701	(698.0 ± 7.1)	474	(495.1 ± 4.9)	726	(750.7 ± 7.3)
$\nu^* \to \nu \mathrm{Z}^0$			331	(363.4 ± 4.7)		
			Pair production			
$\ell^* \to \ell\gamma$	2	(3.42 ± 0.52)	2	(1.12 ± 0.08)	7	(6.89 ± 0.63)
$\ell^* \to \nu W$ (hadr.)			1125	(1182.7 ± 8.1)		
$\ell^* \to \nu W$ (semilep.)			653	(666.6 ± 5.1)		
$\nu^* \to \nu\gamma$			13	(8.97 ± 0.55)		
$\nu^* \to \ell W$	10	(9.23 ± 0.57)	2	(3.76 ± 0.31)	55	(48.4 ± 1.4)

Theoretical errors on the computed cross-sections translate into uncertainties on the expected number of background events, typically less than 2% [23].

At the event generator level, the simulated distributions of the kinematic variables used in the event selection may not match the distributions for the data, due either to an imperfect description of the detector or of the background processes at the event generation level. Possible effects on the selected number of simulated events were estimated by studying the change in the ratio between the number of selected events in the data and simulated background when varying each selection cut around the nominal value. The most relevant variables used in the event selection were changed as follows: the photon polar angle was varied by $\pm 5^\circ$; the cut in the lepton energy was changed by ± 5 GeV; the jet-jet acoplanarity cut was varied by $\pm 5^\circ$; the limits in the jet-jet invariant mass window were changed by ± 10 GeV. In each topology the contributions from the different selection cuts were added in quadrature. The total systematic uncertainty from the event selection

Table 6. Selection efficiencies for the different excited lepton flavours and decay channels, in the single (*top*) and pair (*bottom*) production modes. Efficiencies are quoted for excited lepton masses of $m_{L^*} = 125, 150$ and $200\,\mathrm{GeV}/c^2$ in the single production and $m_{L^*} = 100\,\mathrm{GeV}/c^2$ in the pair production, at $\sqrt{s} = 206$ GeV. The relative statistical errors range between 3% and 8%, depending on the channel

Channel	Excited-lepton flavour e	μ	τ
		Single production	
$\ell^* \to \ell\gamma$	0.39, 0.43, 0.40	0.58, 0.58, 0.61	0.29, 0.30, 0.23
$\ell^* \to \nu W$	0.20, 0.24, 0.33	0.32, 0.32, 0.33	0.24, 0.25, 0.43
$\ell^* \to \ell Z$	0.05, 0.04, 0.20	0.39, 0.39, 0.42	0.16, 0.16, 0.20
$\nu^* \to \nu\gamma$		0.0, 0.0, 0.37	
$\nu^* \to \ell W$	0.27, 0.31, 0.34	0.27, 0.34, 0.34	0.16, 0.19, 0.18
$\nu^* \to \nu Z$		0.30, 0.31, 0.41	
		Pair production	
$\ell^* \to \ell\gamma$	0.38	0.51	0.17
$\ell^* \to \nu W$ (hadr.)		0.22	
$\ell^* \to \nu W$ (semilep.)		0.16	
$\nu^* \to \nu\gamma$		0.53	
$\nu^* \to \ell W$	0.28	0.42	0.13

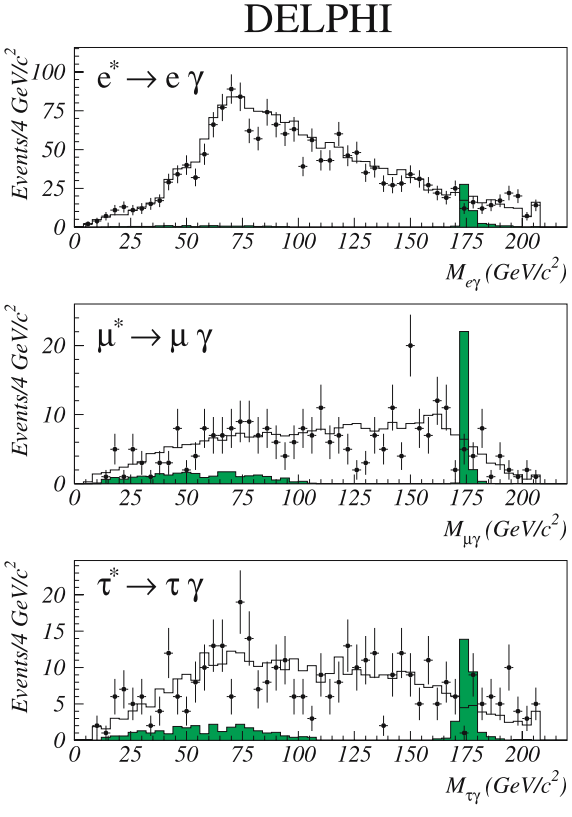

Fig. 7. Lepton-photon invariant masses for the selected candidates in the $\ell^* \to \ell\gamma$ channels. Events selected in all relevant final-state topologies at all centre-of-mass energies were added. For events from the $\ell\ell\gamma$ final-state topology the two possible $\ell\gamma$ combinations are shown. The *dots* show the data and the *white histograms* show the expected SM background. The *shaded histograms* show the expected signal distributions at $\sqrt{s} = 206$ GeV with $m_{\ell^*} = 175\,\mathrm{GeV}/c^2$, using an arbitrary normalization

cuts ranged between 5% and 8%, depending on the topology considered. These were taken as an estimate of the contribution from the analysis cuts to the systematic error on the background expectation. The systematic uncertainties on the signal selection efficiencies due to the selection cuts were assumed to be equal to and fully correlated with the errors estimated above for the background.

The statistical errors on the background and signal efficiencies, due to the limited Monte Carlo statistics, were taken as uncorrelated systematic uncertainties.

An additional source of systematic error on the signal efficiency is due to the description of initial-state radiation (ISR) effects at the event generator level. Single excited-lepton events were generated with collinear ISR only. As long as ISR photons are emitted below the DELPHI acceptance, this results only in a small change in the event kinematics, with low impact on the signal selection efficiency. However, if the ISR photon was detected, the event topology would be different from the topologies considered in the analysis, resulting in a smaller efficiency for the signal. This effect was estimated using $e^+e^- \to e^+e^-$ and $e^+e^- \to \mu^+\mu^-$ events simulated at centre-of-mass energies from 189 GeV to 208 GeV. For each centre-of-mass energy the ratio between the total number of generated events and the number of events with a photon with $E_\gamma > 5$ GeV and $\theta_\gamma > 3^\circ$ was obtained. By averaging over all centre-of-mass energies an efficiency correction factor $k = 0.90 \pm 0.02$ was obtained. The error on k was taken as an independent contribution to the systematic uncertainty of the signal efficiencies.

The systematic uncertainties discussed in this section were included in the computation of the exclusion limits.

5.2 Limits

Limits at 95% confidence level (CL) were computed using the modified frequentist likelihood ratio method described

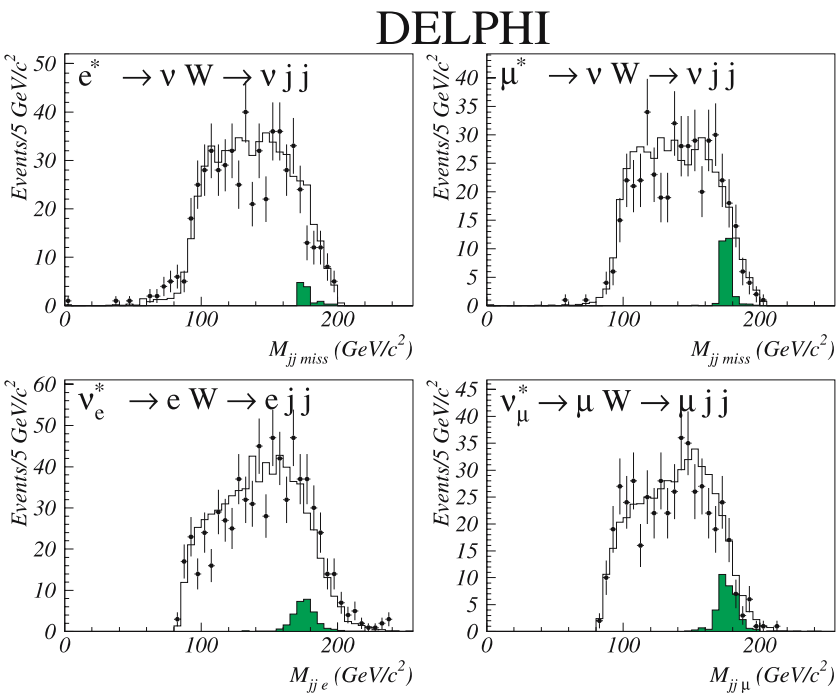

Fig. 8. Invariant mass distributions for the selected candidates in the $\ell^* \to \nu W$ (*top*) and $\nu^* \to \ell W$ (*bottom*) channels. Events selected in the $jj\ell$ topology at all centre-of-mass energies were added. The *dots* show the data and the *white histograms* show the expected SM background. The *shaded histograms* show the expected signal distributions at $\sqrt{s} = 206$ GeV with $m_{L^*} = 175\,\mathrm{GeV}/c^2$, using an arbitrary normalization

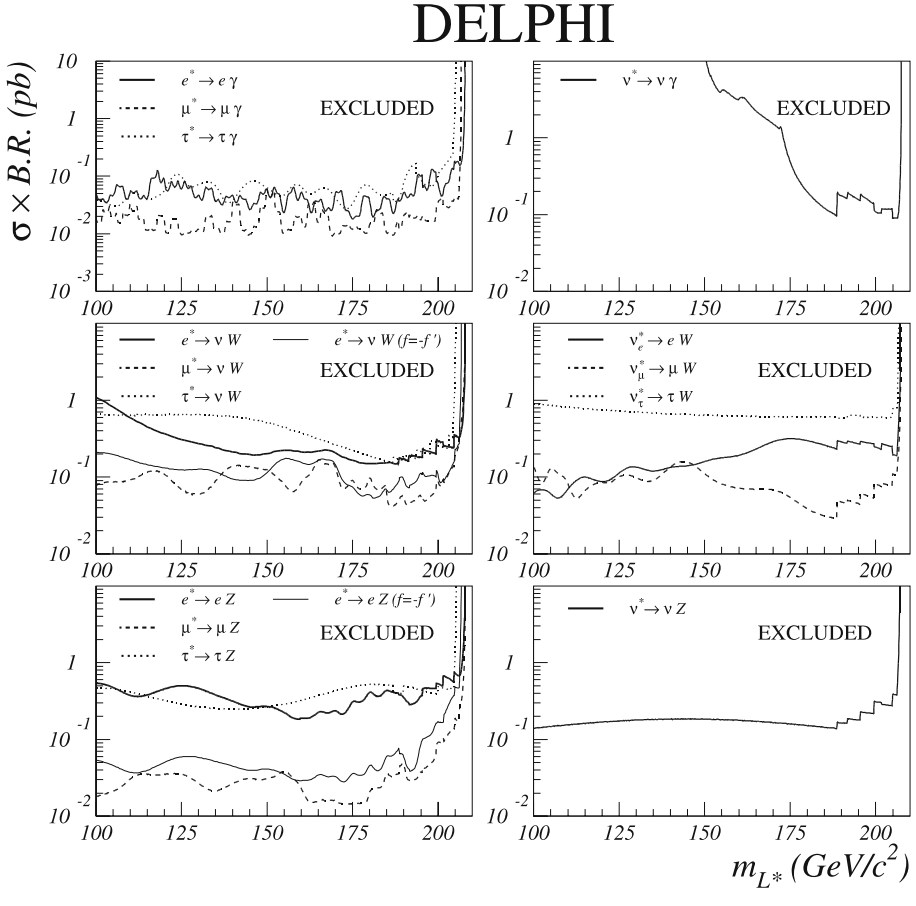

Fig. 9. Results on the single-production search of charged and neutral excited leptons. The *lines* show the upper limits at 95% CL on $\sigma \times \mathrm{BR}$ as a function of the particle mass, for each lepton flavour and decay mode

in [24]. This method is well suited both for the combination of different search channels and for the inclusion of mass information. Searches in each topology at each centre-of-mass energy are treated as independent channels. Whenever the mass of the particle being searched for can be reconstructed, the PDF for a given signal mass hypothe-

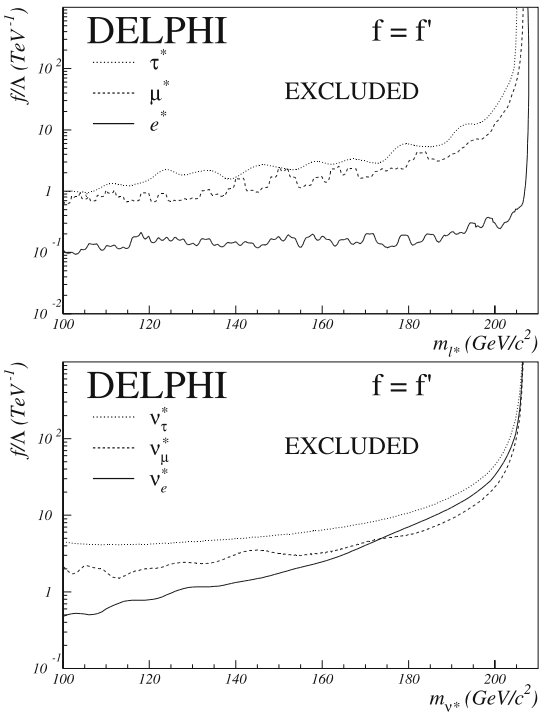

Fig. 10. Results on single-production search of excited charged (*upper plot*) and neutral (*lower plot*) leptons assuming $f = f'$. The *lines* show the upper limits at 95% CL on f/Λ as a function of the excited-lepton mass

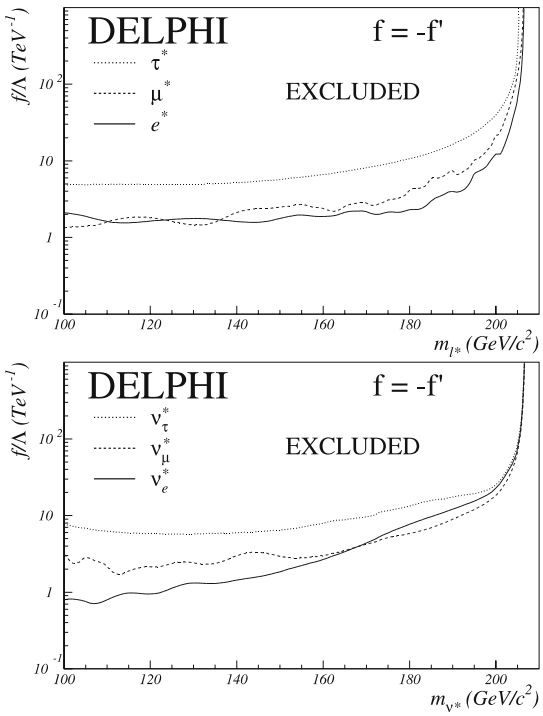

Fig. 11. As Fig. 10, but for $f = -f'$

sis is assumed to be Gaussian with mean value equal to the tested signal mass and standard deviation equal to the signal mass resolution. For channels where the excited-lepton mass is not reconstructed, all selected events are candidates for all signal mass hypotheses. In the $\ell^*\ell^* \to \nu\mathrm{W}\nu\mathrm{W}$ channel, for which a discriminant analysis was performed, the PDFs of the likelihood ratio obtained at each signal mass hypothesis are used.

From the single-production search results, upper limits on the production cross-section multiplied by the decay branching ratio ($\sigma \times \mathrm{BR}$), as a function of the mass, were derived for each excited-lepton type and decay mode, as shown in Fig. 9. As already discussed, the kinematics of single e^* production is sensitive to the contribution from t-channel γ exchange, with impact on the selection efficiencies. The e^* limits were thus computed using the selection efficiencies obtained with $f = f'$ and $f = -f'$. With $f = -f'$ the e^* decay to a photon is forbidden. For the other excited-lepton flavours the selection efficiencies do not depend on the f and f' assignments. The limits on $\sigma \times \mathrm{BR}$ can thus be interpreted in broader compositeness scenarios.

The cross-section for single excited-lepton production is a function not only of m_{L^*} but also of the coupling parameter f/Λ. The pair-production cross-section is a function of m_{L^*} only. Upper limits on f/Λ as a function of m_{L^*} and lower limits on m_{L^*} were derived from the single- and pair-production searches respectively, by combining the results in the various decay modes. The dependence of the decay BR's and production cross-sections on m_{L^*} as given in [3] were assumed. The production cross-sections were computed taking into account initial-state radiation effects.

Figures 10 and 11 show the limits on f/Λ as a function of m_{L^*} for $f = f'$ and $f = -f'$, respectively. The lower limits on the excited-lepton masses are given in Table 7 for the two scenarios. It should be noted that the search for charged excited leptons yielded similar results in both scenarios. In the $f = -f'$ case, although a poorer efficiency *vs* purity was obtained in the total number of selected events, the use of the discriminant analysis was crucial to keep the signal sensitivity comparable with the $f = f'$ case.

Compositeness can also be probed at LEP through the process $e^+e^- \to \gamma\gamma(\gamma)$. The additional contribution of the t-channel exchange of a virtual excited electron to the $e^+e^- \to \gamma\gamma(\gamma)$ cross-section leads to a change in the angular distribution of the final-state photons with respect to the SM prediction. This effect depends on the excited electron mass m_{e^*} and on the $ee^*\gamma$ coupling. The results presented in [25] were used to complement the direct searches for the excited electron in the mass region above the kinematic limit for ee^* production. Figure 12 shows the upper limit on f/Λ for the single production of excited electrons with $f = f'$, obtained by taking the best limit of the direct search (Fig. 10(a)) and the indirect search results, thus extending the excluded region beyond the kinematic limit.

6 Summary

The data collected by DELPHI at $\sqrt{s} = 189 - 209\,\mathrm{GeV}$, corresponding to an integrated luminosity of $598.7\,\mathrm{pb}^{-1}$, were analysed to search for excited leptons decaying

Table 7. Lower limits (in GeV/c^2) at 95% CL on the excited-lepton masses obtained from the pair-production searches

	e^*	μ^*	τ^*		ν_e^*	ν_μ^*	ν_τ^*
$f = f'$	103.1	103.2	102.7	$f = f'$	101.9	103.2	94.2
$f = -f'$	101.0	101.0	101.0	$f = -f'$	101.9	102.2	101.9

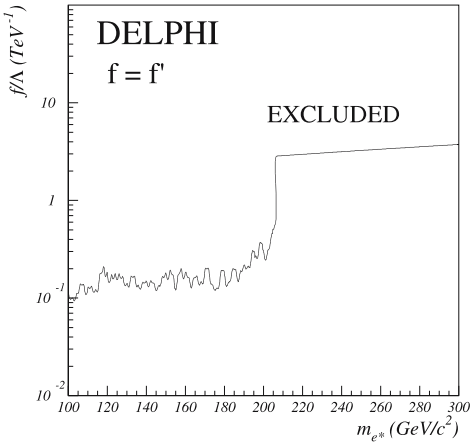

Fig. 12. Combined limit on excited electron production for $f = f'$ from direct and indirect searches. The *line* shows the upper limit at 95% CL on f/Λ. Up to the kinematic limit the result is dominated by the direct search for single production. For masses above the kinematic limit the result stems from the indirect search of excited electron contribution to the process $e^+e^- \to \gamma\gamma$ as described in [25]

promptly through γ, Z^0 or $W^\pm$ emission. No evidence for excited-lepton production was observed. Limits on the model parameters were derived in two scenarios: $f = f'$ and $f = -f'$. From the single-production search upper limits on f/Λ as a function of m_{L^*} were set, as shown in Figures 10, 11 and 12. The search for pair production of excited leptons resulted in mass limits in the range 94–103 GeV/c^2 depending on the excited-lepton type and the assumed scenario for the coupling parameters, as quoted in Table 7. These limits are close to the kinematic limit for all charged (neutral) excited leptons in the $f = f'$ ($f = -f'$) scenario. Model independent upper bounds on $\sigma \times \mathrm{BR}$ were also derived for each excited-lepton flavour and decay channel, thus allowing for interpretations in broader compositeness scenarios.

Acknowledgements. We are greatly indebted to our technical collaborators, to the members of the CERN-SL Division for the excellent performance of the LEP collider, and to the funding agencies for their support in building and operating the DELPHI detector. We acknowledge in particular the support of Austrian Federal Ministry of Education, Science and Culture, GZ 616.364/2-III/2a/98, FNRS–FWO, Flanders Institute to encourage scientific and technological research in the industry (IWT), Belgium, FINEP, CNPq, CAPES, FUJB and FAPERJ, Brazil, Czech Ministry of Industry and Trade, GA CR 202/99/1362, Commission of the European Communities (DG XII), Direction des Sciences de la Matière, CEA, France, Bundesministerium für Bildung, Wissenschaft, Forschung und Technologie, Germany, General Secretariat for Research and Technology, Greece, National Science Foundation (NWO) and Foundation for Research on Matter (FOM), The Netherlands, Norwegian Research Council, State Committee for Scientific Research, Poland, SPUB-M/CERN/PO3/DZ296/2000, SPUB-M/CERN/PO3/DZ297/2000, 2P03B 104 19 and 2P03B 69 23(2002-2004), FCT - Fundação para a Ciência e Tecnologia, Portugal, Vedecka grantova agentura MS SR, Slovakia, Nr. 95/5195/134, Ministry of Science and Technology of the Republic of Slovenia, CICYT, Spain, AEN99-0950 and AEN99-0761, The Swedish Research Council, Particle Physics and Astronomy Research Council, UK, Department of Energy, USA, DE-FG02-01ER41155, EEC RTN contract HPRN-CT-00292-2002.

References

1. F. Boudjema et al., CERN Report CERN-89-08, ed. by G. Altarelli, R. Kleiss, C. Verzegnassi (1989), p. 185; G.F. Giudice et al., CERN Report CERN-96-01, ed. by G. Altarelli, T. Sjöstrand, F. Zwirner (1996), p. 463; and referencees therein
2. K. Hagiwara, D. Zeppenfeld, S. Komamiya, Zeit. Phys. C **29**, 115 (1985)
3. F. Boudjema, A. Djouadi, J.L. Kneur, Zeit. Phys. C **57**, 425 (1993)
4. A. Djouadi, Zeit. Phys. C **63**, 317 (1994)
5. DELPHI Collaboration, P. Abreu et al., Phys. Lett. B **380**, 480 (1996)
6. DELPHI Collaboration, P. Abreu et al., Eur. Phys. J. C **8**, 41 (1999)
7. ALEPH Collaboration, R. Barate et al., Eur. Phys. J. C **4**, 571 (1998); ALEPH Collaboration, D. Buskulic et al., Phys. Lett. B **385**, 445 (1996); L3 Collaboration, P. Achard et al., Phys. Lett. B **568**, 23 (2003); L3 Collaboration, M. Acciarri et al., Phys. Lett. B **502**, 37 (2001); OPAL Collaboration, G. Abbiendi et al., Phys. Lett. B **544**, 57 (2002); OPAL Collaboration, G. Abbiendi et al., Eur. Phys. J. C **14**, 73 (2000)
8. H1 Collaboration, C. Adloff et al., Phys. Lett. B **548**, 35 (2002); H1 Collaboration, C. Adloff et al., Phys. Lett. B **525**, 9 (2002); H1 Collaboration, C. Adloff et al., Eur. Phys. J. C **17**, 567 (2000); ZEUS Collaboration, S. Chekanov et al., Phys. Lett. B **549**, 32 (2002); ZEUS Collaboration, J. Breitweg et al., Zeit. Phys. C **76**, 631 (1997)
9. DELPHI Collaboration, P. Aarnio et al., Nucl. Instr. Methods A **303**, 233 (1991); DELPHI Collaboration, P. Abreu et al., Nucl. Instr. Methods A **378**, 57 (1996)
10. S. Jadach, B.F.L. Ward, Z. Wąs, Comput. Phys. Comm. **130**, 260 (2000)

11. S. Jadach, B.F.L. Ward, Z. Wąs, Comput. Phys. Comm. **66**, 276 (1991)
12. S. Jadach, W. Placzek, B.F.L. Ward, Phys. Lett. B **390**, 298 (1997)
13. E. Accomando, A. Ballestrero, Comput. Phys. Comm. **99**, 270 (1997); E. Accomando, A. Ballestrero, E. Maina, Comput. Phys. Comm. **150**, 166 (2003)
14. T. Sjöstrand et al., Comput. Phys. Comm. **135**, 238 (2001); T. Sjöstrand, Comput. Phys. Comm. **82**, 74 (1994); T. Sjöstrand, Preprint CERN-TH/7112-93 (1993)
15. F.A. Berends, P.H. Daverveldt, R. Kleiss, Comput. Phys. Comm. **40**, 271 (1986)
16. F.A. Berends, P.H. Daverveldt, R. Kleiss, Comput. Phys. Comm. **40**, 285 (1986)
17. D. Karlen, Nucl. Phys. B **289**, 23 (1987)
18. F. Berends, R. Kleiss, Nucl. Phys. B **186**, 22 (1981)
19. DELPHI Collaboration, J. Abdallah et al., Eur. Phys. J. C **35**, 313 (2004)
20. S. Catani et al., Phys. Lett. B **269**, 432 (1991)
21. DELPHI Collaboration, J. Abdallah et al., Eur. Phys. J. C **38**, 395 (2005)
22. DELPHI Collaboration, P. Abreu et al., Eur. Phys. J. C **2**, 581 (1998)
23. G. Altarelli, T. Sjöstrand, F. Zwirner (Eds.) CERN Report 96-01, vol.2 (1996); S. Jadach, G. Passarino, R. Pittau (Eds.) CERN Report 2000-009 (2000)
24. A.L. Read, CERN Report 2000-005, ed. by F. James, L. Lyons, Y. Perrin (2000), p 81
25. DELPHI Collaboration, J. Abdallah et al., Eur. Phys. J. C **37**, 405 (2004)